DESIGN CONCERNS FOR TIP-BASED MEASUREMENT TOWARDS PROCESS METROLOGY IN ROLL-TO-ROLL NANOMANUFACTURING

Liam G. Connolly, Barbara Groh, James A. Garcia, and Michael Cullinan
Walker Department of Mechanical Engineering
The University of Texas at Austin
Austin, Texas, USA

INTRODUCTION

Roll-to-roll (R2R) manufacturing as applied to products with micro- and nanometer scale features promises to bring a class of manufactured goods which match or exceed performance of counterparts fabricated with traditional silicon wafer or glass panel based substrates, while also possessing unique mechanical properties and pointedly lowered processing cost [1]–[6]. From functional materials, flat optics, and even integrated circuits, the drive for faster, cheaper, and more tightly integrated products has driven intense research focus on enabling R2R fabrication techniques which can successfully make the jump from academic experimentation to high volume manufacturing (HVM) [7]–[14]. While lab- and pilot-scale fabrication has been demonstrated, there exists a significant hurdle to widespread adoption and further advancement of these manufacturing techniques, specifically for nanometer scale patterns — the metrology problem [15]–[17].

The drivers of profitable HVM of nanofeatured products and devices can be distilled down to two primary factors, yield and throughput. Figure 1 demonstrates the throughput and thus processing cost advantage compared to wafer based manufacturing due to these factors [18]. However, it is an open issue as to whether yields may rise to a high enough level to deliver on these lofty goals towards HVM. While R2R manufacturing holds a major throughput advantage compared to more highly adopted silicon wafer or glass panel based manufacturing processes due to its continuous nature, *make it by the mile* is only a successful strategy if economically sustainable yields can be reached. The major areas of research needed to enable high volume R2R nanomanufacturing as identified by the U.S. National Institute of Standards and Technology include technology for high-throughput alignment, real-time metrology, and closed loop process control. In practice, achieving viable yields is an area of significant difficulty, and as such the task of quickly, precisely, and non-destructively measuring fabricated nanopatterns is an area of great research interest [16], [19].

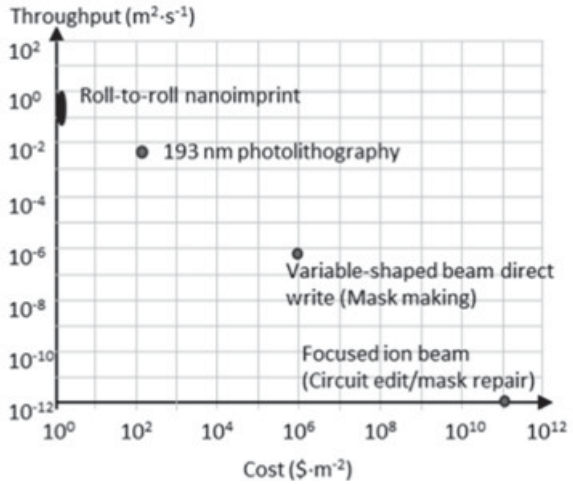

FIGURE 1: Throughput vs. cost in R2R and wafer-based lithography [18]

While a significant proportion of current art in metrology for R2R nanopatterning is relatively recent, with most occurring within the last decade as could be expected of a relatively nascent manufacturing technology, several approaches have been investigated and shown to be effective at specific, and often disparate, measures of performance and efficacy [20]. The techniques vary by the physical phenomena which they use to measure fabricated features in addition to throughput, compatibility with in-line measurement in R2R HVM, and measurement precision. Further, despite the overarching basis of many of these approaches originating from years of development for similar tools in the wafer semiconductor fabrication industry, extension to R2R nanomanufacturing remains a significant challenge.

INITIAL PROTOTYPE

Previous work presented a proof-of-concept prototype apparatus [21] which employs a novel,

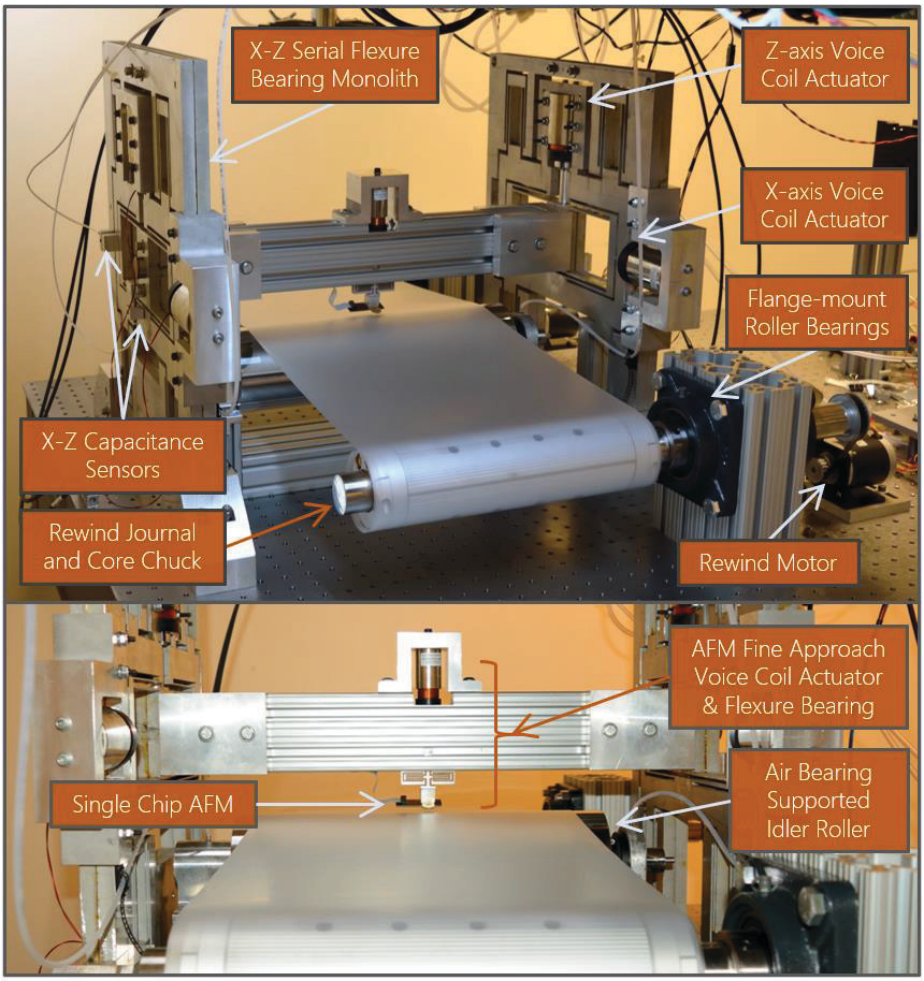

FIGURE 2: Previously presented proof-of-concept prototype tool with major subsystems labeled.

micro-electro-mechanical system (MEMS) based atomic force microscope (AFM), the single chip AFM (sc-AFM, ICSPI Corp.), to the problem of R2R process metrology. This design choice allows for nm-scale tip-based measurement in a volume and mechanical environment which would normally be incongruent to the implementation of a traditional AFM tool. The proof-of-concept prototype employed linear double parallelogram flexure mechanism (DPFM) bearings to position a mechanical structure in the X (web direction) and Z (vertical) directions such that the sc-AFM could be used to "step-and-scan" over nanofeatured structures produced on thin, R2R substrates. Figure 3 shows an example of the measurement results from the sc-AFM (right) in comparison to a traditional table-top SEM micrograph (left).

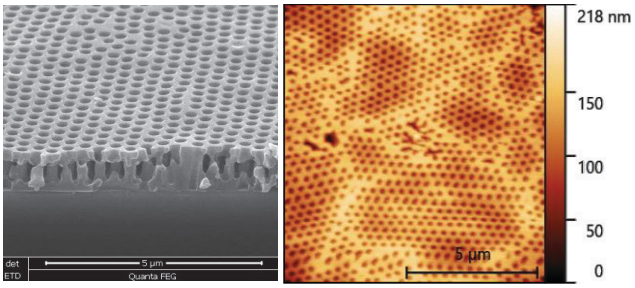

FIGURE 3: SEM micrograph (left) and sc-AFM scan result of polymeric, nanometer scale holes fabricated through R2R-capable interference lithography.

IMPROVED PROTOTYPE

To refine the proof-of-concept system towards a more precise implementation of the previously demonstrated architecture, in addition to the overall goal of moving from step-and-scan measurement to quasicontinuous measurement with the sc-AFM probe, e.g. a mode of operation such that the R2R substrate does not require stoppage for measurement. This capability would thusly improve throughput and compatibility with R2R HVM. A redesign of the various subsystems was undertaken towards this goal. To enable high speed tracking of the top surface of the sample

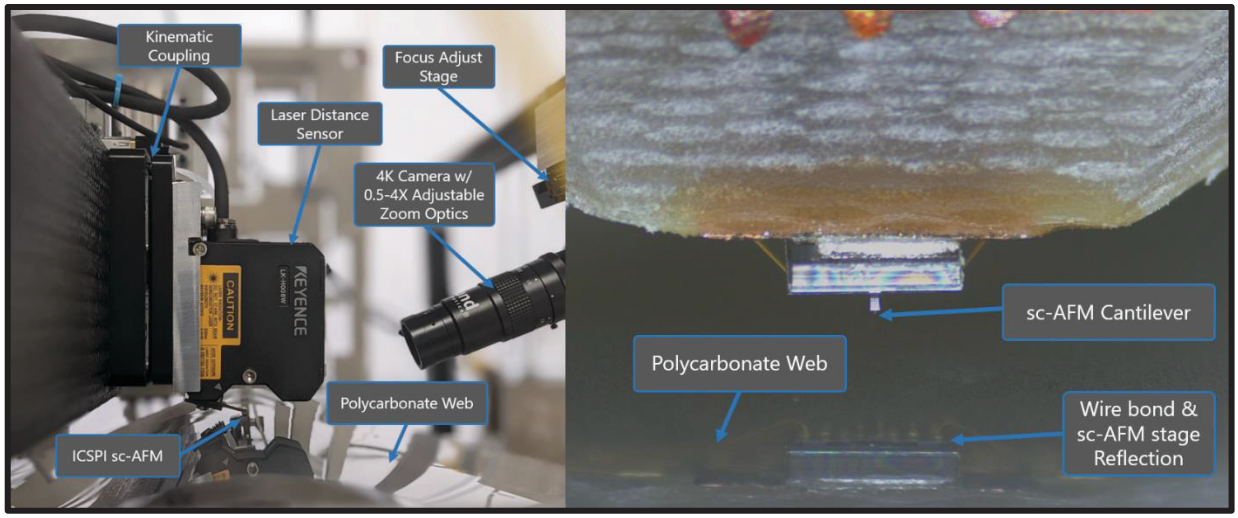

FIGURE 4: Side-view of the upgraded tool's measurement sensor module (left) and micrograph from the on-tool optical monitoring system (right) with major sub-systems labelled.

web, a 5 nm repeatability laser triangulation distance sensor (Keyence LK-H008W) is added adjacent to the sc-AFM probe such that active feedback control can be implemented to lock on to a specific tip-sample separation distance during scans and compensate for any roller runout, geometric eccentricity, and any web thickness nonuniformities. As this design is only intended for use with a single sc-AFM, the fine approach DPFM bearing and linear voice coil motor shown in the previously presented work were removed to minimize compliance in the mechanical path between the sc-AFM and sample. A process monitoring camera with 4K resolution and 0.5X to 4X adjustable zoom optics (Edmund Optics VZM 400i) is also added for remote monitoring. To maximize the specific stiffness, the structure's stiffness normalized to mass, of the gantry the previous prototype's aluminum extrusion was replaced with a carbon fiber reinforced polymer (CRFP) structure with bonded 6061 aluminum end caps. The CRFP in this case is primarily made with unidirectional carbon fibers to maximize the bending stiffness of the gantry arm. A screw-locking, kinematic coupling (Newport BKL-4) is then attached to a machined flat on the CRFP gantry arm by means of bonded, threaded inserts to facilitate fast and easy sc-AFM tip exchange without significant realignment of the system. Figure 4 details a side profile view of this sc-AFM probe mounting arrangement in addition to a micrograph from the integrated imaging system.

While the initial prototype tool utilized capacitance probe based sensing to measure the position of each motion axis, in order to fully take advantage of the maximum range of the flexure mechanisms, a new sensing solution was required. Whereas the capacitance gauges could only reliably measure ~250 µm, a new system of Fabry-Perot interferometric distance sensors (Attocube FPS3010) is implemented with mm-scale range well beyond the maximum displacement of either the Z- or X-axis flexure stages, and a maximum stage velocity of 2 m/s. Further, the bandwidth of the interferometer sensing system exceeds 100 kHz when interfacing with the FPGA control system through a custom, digital, high-speed serial communication protocol compared to the ~5 kHz bandwidth of the previous sensors in addition to eliminating the inherent electromagnetic interference present in analog voltage measurements. As only three channels are available, both sides of the X-axis flexure stage positions are measured but the Z-axis is sensed on only one side of the system. For the flexure stage with two channels, a perpendicular, chromium carbide reflecting cube (Starrett-Webber, 5 arc-sec perpendicularity, λ/20 flatness) is used. On the single-measurement side, a small 0.5" diameter protected gold first surface mirror is employed with λ/10 flatness.

To reduce any vibration-inducing slip between the moving web and the idler roller on which sc-AFM scans are taken, a new light weight and high stiffness idler roller with low angular moment of inertia was fabricated. This roller consists of a 6" diameter CRFP drum with billet stainless steel hubs bonded to each end. Attached to these hubs are stainless steel bearing journals for the same combination of radial air bushing and thrust air bearing used in the initial prototype, albeit with improved billet

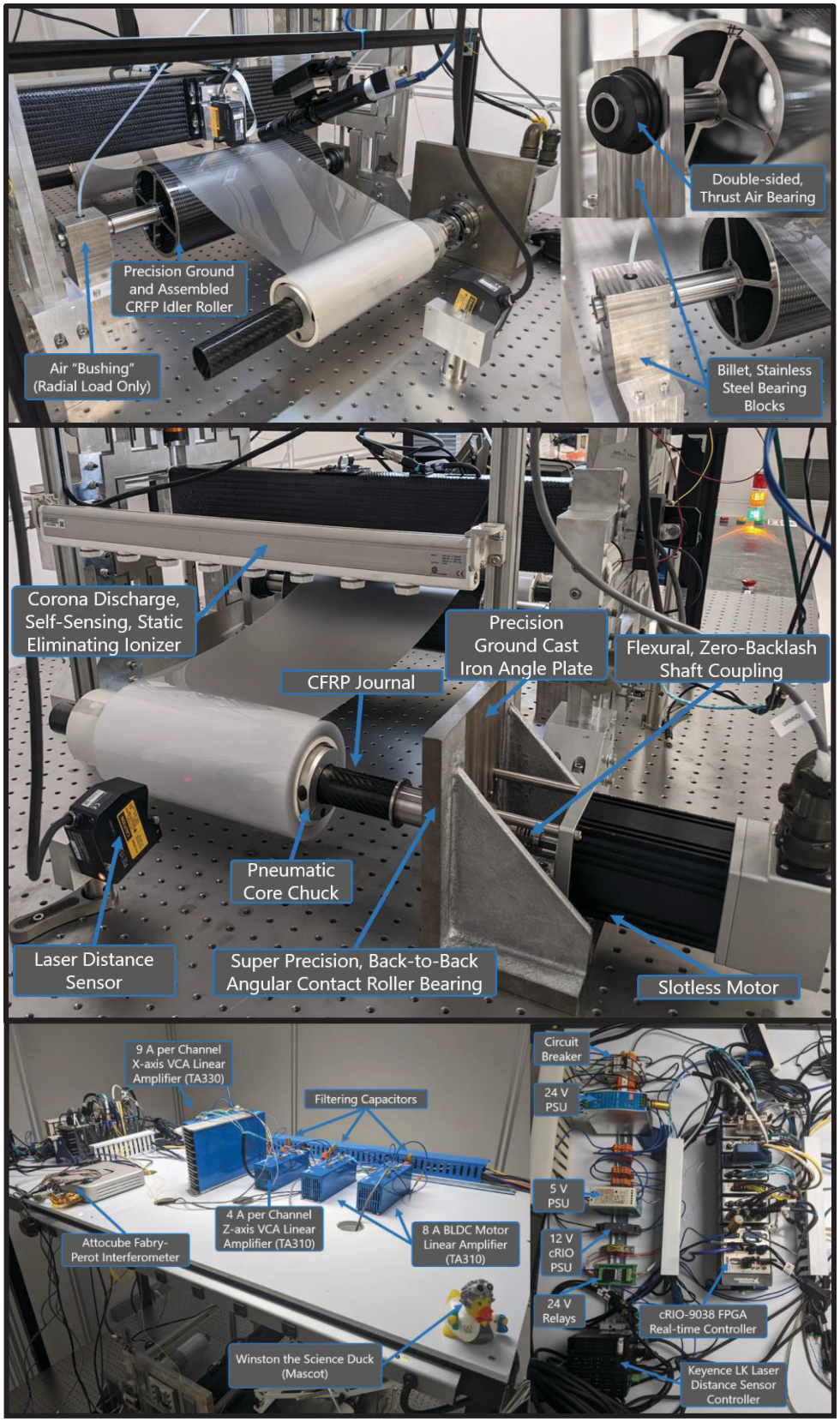

FIGURE 5: Upgraded carbon fiber metrology roller and stainless steel air bearing housings (Top) , wind stand architecture with improved actuator, motion bearings, and sensing (middle), and control and power electronic systems with major components highlighted.

stainless steel bearing blocks for increased stiffness and lowered coefficient of thermal expansion. The air bushing is mounted in the housing through a tight-fitting series of fluorocarbon O-rings such that any misalignment due to optical table flatness or angular misalignment is taken up by the compliance of the O-rings. The thrust air bearing is press fit into its respective housing. This improved sub-system is outlined in Figure 5 (top) with the major components labelled.

Upgrades for the web handling sub-system again focus on achieving semicontinuous sc-AFM scanning. To minimize the effect of random errors in linear velocity and tension commands, super precision class cartridge bearings (SKF BEAM 025075-RS) were chosen to replace the low cost, self-aligning roller bearings used in the preliminary prototype tool as shown in Figure 5 (top). By selecting a heavily preloaded, ~1.92 kN, back-to-back bearing architecture, stiffness to both applied moments and web tensioning force is high – 200 Nm/mrad and 790 N/μm respectively. Unlike typical super precision bearings, the only stringent dimensional requirement for the chosen cartridge bearing is the flatness of the mounting plate, easing fabrication difficulty and cost for the wind stand structures. In this case, grey cast iron precision ground angle plates (Shars Tools) with flatness of less than 0.0005” were chosen for both their ease of modification and low cost in addition to the high perpendicularity to aid in alignment between the unwind and rewind stands which are fastened to the optical table breadboard surface, as shown in Figure 5 (middle). Further, instead of relying on initial roll diameters, turn counting, and assumed web thickness to convert from angular velocity and torque to linear web velocity and web tension, high-speed, precision laser triangulation sensors with 100 nm repeatability (Keyence LK-H087) are added to sense roller diameter change from an initially measured value on startup. For the rewind stand which regulates web velocity, a 30,000 period per revolution sine-cosine optical angular encoder (Heidenhain ERP 1080 - 30000) is employed. Additional improvements include the replacement of the inexpensive, brushless DC stepper motors with precision, high-torque slotless, brushless, DC motors (Aerotech BMS280) directly coupled to the wind journals through a stainless steel flexural shaft coupling. In slotless motors, rather than winding coils about iron teeth, a method which saves on manufacturing costs and achieves high torque density, slotless motor coils are either potted in a thermoset polymer such as epoxy or wound about nonmagnetic cores [22]–[24]. While doing so increases costs and lowers overall torque density, it all but eliminates the rotational torque ripple due to the flux channeled by the ferritic teeth of a traditional brushless DC motor

An upgraded cRIO real-time control system with significantly increased FPGA size and resources (National Instruments cRIO-9038) in addition to low noise, 5 kHz bandwidth, linear current transconductance amplifiers to drive both the linear voice coil motors and the rotary slotless BLDC motors (Trust Automation TA310 & TA330) are also added. In this case the amplifier for the X-axis voice coil motors is sized for maximum turnaround throughput during quasicontinuous scanning operations, i.e., high acceleration, with a theoretical limit of ~5 g acceleration (9 A per coil). To support these upgraded power electronics, high reliability, programmable, low-noise switching DC power supplies (TDK-Lambda GenSys and DPP480-48) are implemented as can be seen in Figure 5 (bottom).

Lastly, to eliminate any surface charging effects due to interleave films and the unwinding of the roll of material which might impart a force on the sc-AFM cantilever, and thus skew any measured sample topography from the ground-truth of the sample surface, a cleanroom compatible, self-sensing ionic static eliminator (Keyence SJ-H060A) based on the corona discharge effect from sharp tungsten tips is installed immediately after the unwind stand, as shown in Figure 5 (middle), to minimize and surface charging.

CONCLUSION

This abstract presents the evolution of a proof-of-concept tool to perform tip-based measurements on flexible, nanopatterend substrates in a R2R manner. The goals of this redesign were to improve precision and throughput of the initial prototype tool in addition to enabling future quasicontinuous scanning of R2R substrates, e.g., the implementation of sc-AFM measurement without the need to stop the web as is the case for current step-and-scan measurements. Future work will detail the control architecture used to implement this quasicontinuous scanning method and the measurement results therein.

ACKNOWLEDGMENTS

The authors would like to thank the ICSPI corporation for material support of this research and many informative discussions. This material

is based upon work supported by the National Science Foundation under Cooperative Agreement No. EEC-1160494, and the Graduate Research Fellowship program under Grant No. 2017251210. Any opinions, findings, and conclusions or recommendations expressed in this material are those of the authors and do not necessarily reflect the views of the National Science Foundation or The University of Texas at Austin.

REFERENCES

[1] J. D. Morse, "Nanofabrication Technologies for Roll-to-Roll Processing," *NIST-NNN Workshop*, 2011.

[2] A. Nathan *et al.*, "Flexible electronics: The next ubiquitous platform," *Proceedings of the IEEE*, vol. 100, no. SPL CONTENT, pp. 1486–1517, 2012, doi: 10.1109/JPROC.2012.2190168.

[3] "NextFlex Roadmapping Meeting." Lowell, MA, 2016.

[4] N. Kooy, K. Mohamed, L. T. Pin, and O. S. Guan, "A review of roll-to-roll nanoimprint lithography," *Nanoscale Research Letters*, vol. 9, no. 1, pp. 1–13, 2014, doi: 10.1186/1556-276X-9-320.

[5] Kenneth Carter, "R2R Nanofabrication: A Test Bed Platform for UMass Nanoscale Science Technologies," University of Massachusetts - Amherst, 2011.

[6] J. A. Rogers *et al.*, "Paper-like electronic displays: Large-area rubber-stamped plastic sheets of electronics and microencapsulated electrophoretic inks," *Proceedings of the National Academy of Sciences of the United States of America*, vol. 98, no. 9, pp. 4835–4840, 2001, doi: 10.1073/pnas.091588098.

[7] S. Ahn *et al.*, "Roll-to-roll nanopatterning using jet and flash imprint lithography," 2012, vol. 8323, pp. 83231L-8323–7. [Online]. Available: https://doi.org/10.1117/12.918040

[8] T. R. Andersen *et al.*, "Scalable, ambient atmosphere roll-to-roll manufacture of encapsulated large area, flexible organic tandem solar cell modules," *Energy and Environmental Science*, vol. 7, no. 9, pp. 2925–2933, 2014, doi: 10.1039/c4ee01223b.

[9] M. Bariya *et al.*, "Roll-to-Roll Gravure Printed Electrochemical Sensors for Wearable and Medical Devices," *ACS Nano*, vol. 12, no. 7, pp. 6978–6987, 2018, doi: 10.1021/acsnano.8b02505.

[10] Y. S. Jung, K. Hwang, Y. J. Heo, J. E. Kim, D. Vak, and D. Y. Kim, "Progress in Scalable Coating and Roll-to-Roll Compatible Printing Processes of Perovskite Solar Cells toward Realization of Commercialization," *Advanced Optical Materials*, vol. 6, no. 9, pp. 1–30, 2018, doi: 10.1002/adom.201701182.

[11] G. Kirchner *et al.*, "Toward high volume solution based roll-to-roll processing of OLEDs," *Journal of Materials Research*, vol. 32, no. 12, pp. 2219–2229, 2017, doi: 10.1557/jmr.2017.204.

[12] I.-T. Chen, E. Schappell, X. Zhang, and C.-H. Chang, "Continuous roll-to-roll patterning of three-dimensional periodic nanostructures," *Microsystems & Nanoengineering*, vol. 6, no. 1, p. 22, Dec. 2020, doi: 10.1038/s41378-020-0133-7.

[13] N. Cates *et al.*, "Roll-to-roll nanoimprint lithography using a seamless cylindrical mold nanopatterned with a high-speed mastering process," *Nanotechnology*, 2021, doi: 10.1088/1361-6528/abd9f1.

[14] C.-H. Chang *et al.*, "From Two-Dimensional Colloidal Self-Assembly to Three-Dimensional Nanolithography," *Nano Letters*, vol. 11, no. 6, pp. 2533–2537, Jun. 2011, doi: 10.1021/nl2011824.

[15] H. Subbaraman, X. Lin, X. Xu, A. Dodabalapur, L. J. Guo, and R. T. Chen, "Metrology and Instrumentation Challenges with High-rate, Roll-to-Roll Manufacturing of Flexible Electronic Systems," *Instrumentation, Metrology, and Standards for Nanomanufacturing, Optics, and Semiconductors VI*, vol. 8466, p. 846603, 2012, doi: 10.1117/12.940778.

[16] U. D. of Energy, "Quadrennial technology review: An assessment of energy technologies and research opportunities (September)," US Department of Energy Washington, DC, 2015.

[17] C. Daniel, D. Wood III, G. Krumdick, M. Ulsh, V. Battaglia, and F. Crowson, "Roll-to-Roll Advanced Materials Manufacturing DOE Laboratory Collaboration - FY2018 Final Report," Oak Ridge National Lab. (ORNL), Oak Ridge, TN (United States), ORNL/SPR-2019/1066, Jan. 2019. doi: https://doi.org/10.2172/1502542.

[18] J. A. Liddle and G. M. Gallatin, "Nanomanufacturing: A Perspective," *ACS Nano*, vol. 10, no. 3, pp. 2995–3014, 2016, doi: 10.1021/acsnano.5b03299.

[19] X. Lin *et al.*, "Towards Realizing High-Throughput, Roll-to-Roll Manufacturing of Flexible Electronic Systems," *Electronics*, vol. 3, no. 4, pp. 624–635, Nov. 2014, doi: 10.3390/electronics3040624.

[20] Z. Ghaznavi, "Roll-to-roll nanofabrication process for flexible Cu metal mesh transparent conducting electrodes," Thesis, 2019. doi: 10.26153/tsw/12397.

[21] L. G. Connolly, T.-F. Yao, A. Chang, and M. Cullinan, "A tip-based metrology framework for real-time process feedback of roll-to-roll fabricated nanopatterned structures," *Precision Engineering*, vol. 57, pp. 137–148, May 2019, doi: 10/gmdbc6.

[22] Yongxiao Chen, Jianxin Shen, and Zemin Fang, "Topology and preliminary design of slotless brushless DC motor," in *1997 IEEE International Electric Machines and Drives Conference Record*, May 1997, p. WB2/7.1-WB2/7.3. doi: 10.1109/IEMDC.1997.604311.

[23] J. Seo, J. Kim, I. Jung, and H. Jung, "Design and Analysis of Slotless Brushless DC Motor," *IEEE Transactions on Industry Applications*, vol. 47, no. 2, pp. 730–735, Mar. 2011, doi: 10.1109/TIA.2010.2091611.

[24] N. Bianchi, S. Bolognani, and F. Luise, "High Speed Drive Using a Slotless PM Motor," *IEEE TRANSACTIONS ON POWER ELECTRONICS*, vol. 21, no. 4, p. 9, 2006, doi: 10.1109/TPEL.2006.876824.